Experimental Investigation on Effects of Various Factors on Very High Cycle Fatigue Property for Spring Steels

Taku Miura[1] , Tatsuo Sakai[2*], Takayuki Sakakibara[3], Shingo Mimura[3] Takanori Kuno[3], Shoichi Kikuchi[2] and Akira Ueno[2]

[1]Graduate School of Science and Engineering, Ritsumeikan University, Kusatsu, Shiga, 525-8577 Japan
[2] College of Science and Engineering, Ritsumeikan University, Kusatsu, Shiga, 525-8577 Japan
[3] Research & Development Division, Chuo Spring Co., Ltd., Miyoshi, Nishikamo, Aichi, 470-0225 Japan
* Corresponding author: sakai@se.ritsumei.ac.jp

Abstract In order to investigate the effects of hardness, residual stress and loading type on the fatigue property for spring steel(SUP7), two kinds of tempering temperature, three kinds of surface finishing (grinding, electrolytic polishing and shot-peening) and two kinds of fatigue test (rotating bending and axial loading) were accepted. Specimens in harder (lower tempering temperature) series showed higher fatigue limit; however, those in shot-peened series showed approximately same fatigue limit as grinding finished series, although the former has compressive residual stress higher than that in the latter. In the case of same tempering temperature and surface finishing, specimens in rotating bending series showed higher fatigue limit comparing with the axial loading. This fact can be attributed to the difference of critical volume participating in the crack initiation. Fracture surfaces of all the failed specimens were carefully observed by a scanning electron microscope(SEM) in order to examine the fracture mode. Two types of interior initiated fracture, with and without inclusion, were found. The latter was found only in axial loading and had granular structure whose angle of slope to the loading direction was 60 degree. In the case of specimens with residual stress (grinding and shot-peening), the depth of interior fracture origin in rotating bending was shallower than that in axial loading. In both grinding and shot-peening series, the crack has initiated beneath the surface layer with compressive residual stress, and, the fatigue limits of these series were thus almost same to each other.

Keywords Spring steel, Very high cycle fatigue, High cleanliness steel, Duplex *S-N* property, Fish-eye

1. Introduction

During the long history of the study on *Fatigue of Metals*, a number of experimental data have been accumulated and a lot of fundamental aspects on the fatigue of metallic materials have been reported by many researchers[1-5]. Among them, one of the most important aspects is the fact that ferrous metals such as structural steels indicate the clear fatigue limit at the number of stress cycles less than 10^7 [1,6]. However, non-ferrous metals such as aluminum alloys have no fatigue limit such that the *S-N* curve tends to decrease continuously in the very long life regime longer than 10^7 cycles[4]. In recent years, practical structures such as railway wheels and rails, offshore structures, energy conversion and transportation systems have been used in a long term, sometimes, beyond their original design lives due to economic and environmental considerations. In such a circumstance, unexpected failures have been reported at stress levels lower than the fatigue limit even for structural components made of ferrous metals being assumed to have a distinct fatigue limit. The fatigue behavior of structural steels in the very high cycle regime longer than 10^7 cycles has become an important subject to ensure the long-term safety of the actual structures in the various areas of industries[4,5].

From this point of view, many researchers have carried out fatigue tests in the very high cycle regime for various kinds of metallic materials in the last decades[4]. Thus, it is known that the high strength steel indicates "duplex *S-N* characteristics" consisting of *S-N* curves for both the surface-initiated fracture and the interior-initiated fracture. According to the conventional works[4], the interior-initiated fracture is usually caused by non-metallic inclusions inside the material in very

high cycle regime. Therefore, if some high cleanliness steel without such inclusions is fabricated, it is supposed that the fatigue fracture caused by the inclusion can be depressed and the corresponding S-N curve is diminished.

From such a viewpoint, a conventional spring steel(SUP7) and a high cleanliness spring steel (SWOSC-V) were prepared mainly supposing the practical application as valve spring for automobile gasoline engine. For both kinds of steels, the rotating bending fatigue tests were performed in the very high cycle regime toward gigacycles. Thus, the fundamental S-N properties for the respective spring steels were experimentally clarified and the effect of the cleanliness on the fatigue property was discussed together with the fatigue fracture mechanism of this steel was also discussed from a view point of fractography.

2. Experimental Procedures

2.1. Material and specimen

Materials used in this study were two different kinds of spring steels; JIS Material Codes of SUP7 and SWOSC-V, respectively. The former is a spring steel for general use for wide variety of usual springs, and the latter is developed for special use as valve spring for automobile gasoline engine. Chemical compositions of these steels were shown in Teble1. In the case of SUP7 steel, the material was firstly oil-quenched at 1173K(900deg.C) /20min, after which it was tempered at each of 723K(450deg.C)/60min and 659K(386deg.C)/60min, respectively. The former is hereafter so-called as “T-450 series”, whereas the latter is as “T-386 series”. Some of T-386 specimens were electrochemically polished (named T-386EP series), and some of T-386EP specimens were further shot-peened(named T-386SP series). All the preparation process of the respective series for SUP7 steel is summarized as a flowchart in Fig.1.

Table 1. Chemical compositions of spring steels

Material	C	Si	Mn	P	S	Cu	Cr	Fe
SUP7	0.6	2.0	0.9	0.014	0.019	—	—	Bal.
SWOSC-V	0.58	1.45	0.69	0.01	0.01	0.02	0.68	Bal.

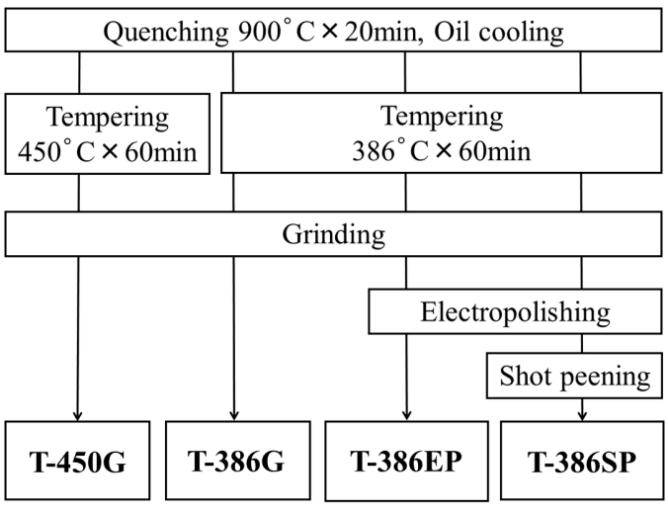

Figure 1. Flowchart of specimen preparation for SUP7 steel

In the case of SWOSC-V steel, the material was oil-quenched at 1123K(850deg.C)/20min and then it was tempered at each of 668K(395deg.C)/60min and 636K (363deg.C)/60min, respectively. Some of 363deg.C-tempered specimens were electrochemically polished, and some of them were shot-peened. In order to distinguish the respective series, notations such as "T-395G series", "T-363G series", "T-363EP series" and "T-363SP series", were introduced similar to the case of SUP7 steel. Preparation process of the respective series for SWOSC-V steel is given in a flowchart in Fig.2.

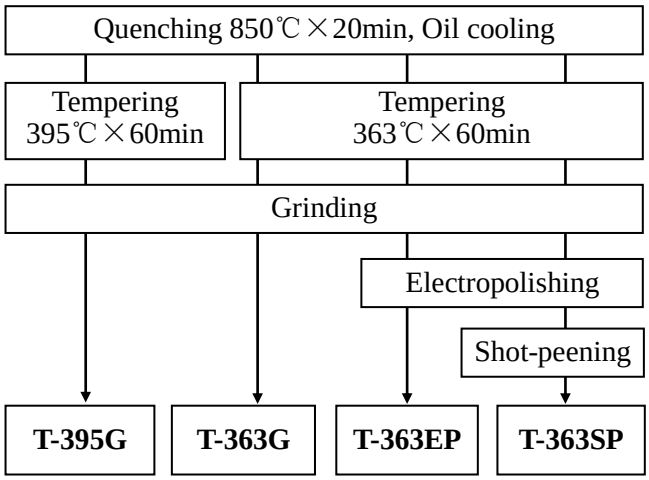

Figure 2. Flowchart of specimen preparation for SWOSC-V steel

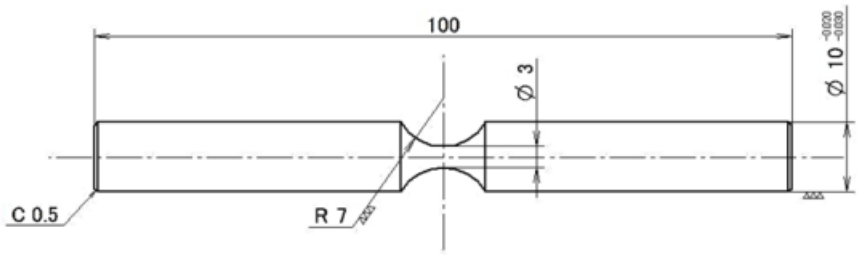

(a) Rotating bending (SUP7)

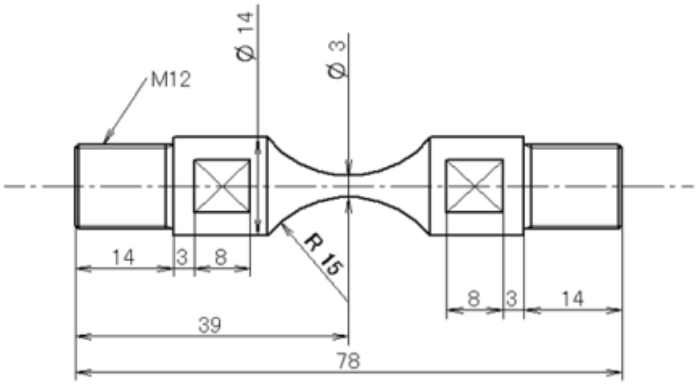

(b) Axial loading

Figure 3. Shape and dimensions of fatigue specimens

Specimens were machined into the shape and dimensions indicated in Fig.3. Figure 3(a) indicates the shape and dimensions of SUP7 specimen for rotating bending. Notch radius of the specimen was 7 mm and the diameter of the critical section was 3mm. The stress concentration factor of this specimen was K_t =1.06 as given by Peterson's handbook. The shape and dimensions of SWOSC-V specimen are quite same as SUP7 except for D=8mm. On the other hand, Fig.3(b) indicates the shape and dimensions of specimen for axial loading. Its notch radius was 15mm and the diameter of the critical section was designed to be 3mm similar to the rotating bending specimen. The stress concentration factor of this specimen was K_t =1.04 from the above handbook. Round notch surface of the specimen was finished by polishing with emery paper of #2000 after the grinding process. Of course, T-386EP series and T-386SP series were tested without such a polishing by emery paper.

In order to characterize the microstructure, the micro-Vickers hardness was measured and the microstructure was observed at cross-section using an optical microscope and a scanning electron microscope (SEM). The distribution of the residual stress was measured at the transverse section of the smallest diameter of the specimen using the X-ray diffraction (XRD). The residual stress distribution in the direction of inside was also measured after electrochemically removing the local surface area.

2.2. Fatigue tests

Photographs of the fatigue testing machines used in this study are shown in Fig.4. The left hand machine was used in rotating bending, whereas the right hand machine was in axial loading. Each of these machines can perform fatigue tests for four specimens simultaneously. The former machine has two spindles driven by an electric motor via a flat belt and each spindle has specimen grips at both ends [5]. The rotating speed of the spindles is 52.5 Hz (3150 rpm), and the stress ratio is given as $R=-1$. The latter machine has four actuators driven by hydraulic power, and the loading frequency is 80Hz. Fatigue tests were carried out at a definite stress ratio of $R=-1$. All the fatigue tests were performed in room atmosphere without any control of temperature and the moisture. After fatigue tests, fracture surfaces were observed by means of SEM and were analyzed by an energy dispersive X-ray spectrometer (EDS).

(a) Rotating bending (b) Axial loading

Figure 4. Multi-type fatigue testing machines used in this study

3. Results and Discussions

3.1. Hardness and residual stress

Vickers hardness of the SUP7 specimens in the respective series was measured and the results are indicated in Fig.5. The hardness of T-386 series is higher than that of T-450 series due to the lower tempering temperature. It is found that the hardness is a little improved by performing the shot-peening. Residual stress distributions are plotted in Fig.6. The residual stress on the specimen surface caused by grinding is in a range of $-400 \approx -500$ MPa, and the residual stress is induced in surface layer within a thickness less than 20 μm. Another typical finding is that distinct compressive residual stress higher than 1000MPa was caused by shot-peening and the depth of the surface layer having such a distinct high residual stress is around 40 μm.

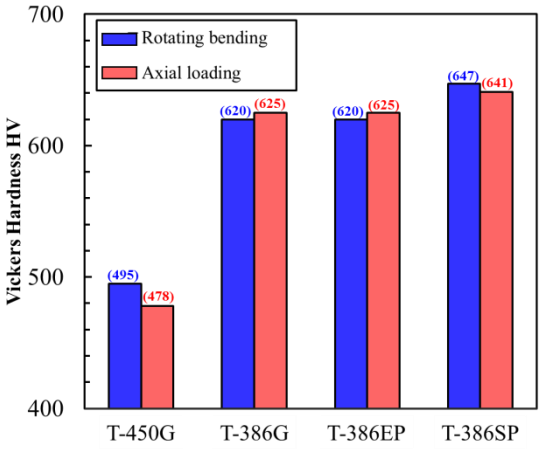

Figure 5. Vickers hardness of the respective series

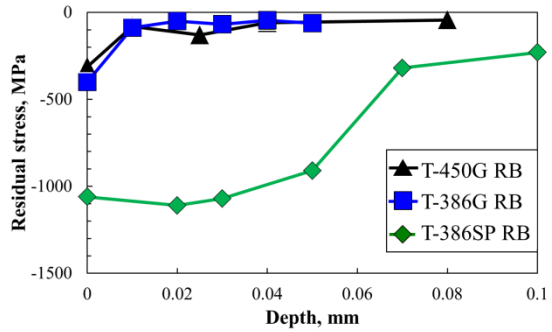

(a) Rotating bending

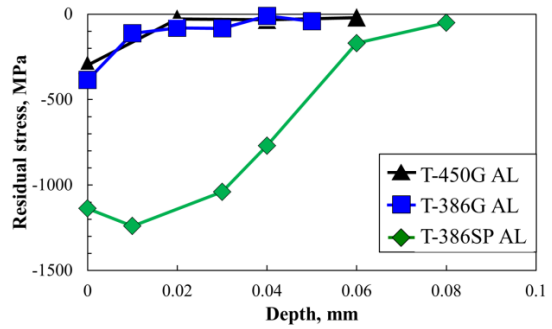

(b) Axial loading

Figure 6. Distributions of residual stress

Vickers hardness of the individual series for SWOSC-V steel is as follows; T-395G series: 584HV, T-363G series: 630HV, T-363EP series: 630HV and T-363SP series: 641HV, respectively. Resulting trend for tempering temperature and shot-peening is quite similar to the results for SUP7 steel. Residual stress for the respective series measured on the specimen surface is as follows; T-395G series: -376MPa, T-363G series: -378MPa, T-363EP series: -31MPa and T-363SP series: -1205MPa, respectively. Thus, residual stress caused by grinding is around 380MPa and this stress is almost entirely removed by electrochemical polishing. However, a distinct compressive residual stress of -1205MPa is produced by performing the shot-peening. This trend is corresponding to the results in Fig.6.

3.2. *S-N* characteristics

Fatigue test results of T-450G and T-386G series for SUP7 steel obtained in rotating bending are plotted as an S-N diagram in Fig.7(a). Every S-N curve was determined by accepting the bilinear

S-N model with fatigue limit in the JSMS standard (JSMS-SD-6-08)[6]. This procedure to determine the S-N curve is entirely common in this paper. It is found that the fatigue limit of T-386G specimen is clearly higher than that of T-450G specimen. This aspect can be attributed to the fact that the hardness of T-386G specimen is much higher than T-450G specimen. Another finding is that interior inclusion initiated fracture is caused only for T-386G specimen. Figure 7(b) indicates the S-N diagram obtained for T-386 specimens in the respective series. The fatigue limit of each series is given as follows; T-386G series: 1025MPa, T-386EP series: 775MPa and T-386SP series: 975MPa, respectively. The marked decrease of the fatigue limit for T-386EP series is caused due to removal of the surface layer having compressive residual stress. It is noted that this decrease of the fatigue limit was almost fully recovered by performing the shot-peening. Paying an attention to the fracture modes, one can find a trend that the interior-induced fracture are observed only for specimens in T-386G and T-386SP series. In the case of T-386EP specimen, the interior-induced fracture was observed for only one specimen.

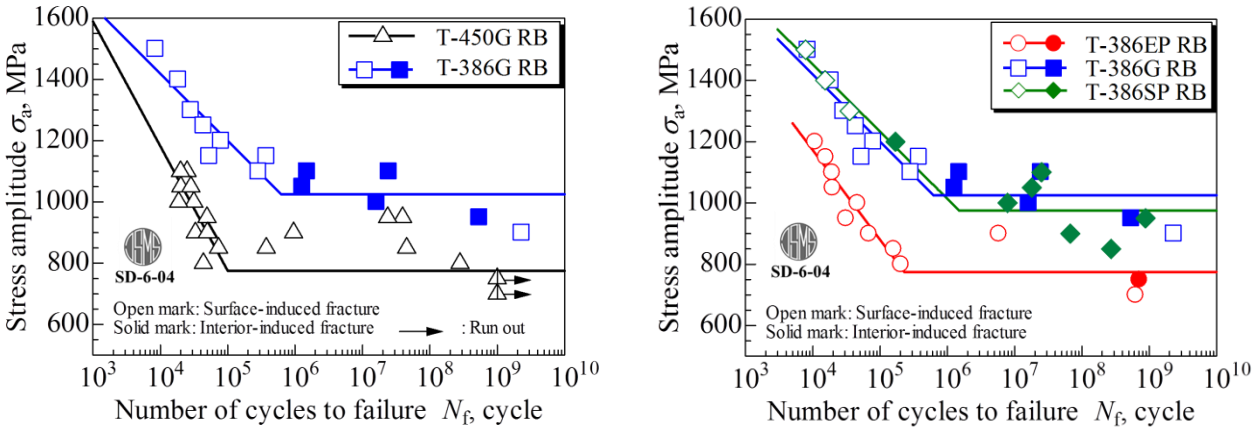

(a) T-450G series and T-386G series (b) Various series of T-386 specimens

Figure 7. S-N diagrams for SUP7 steel in rotating bending

In the next place, fatigue test results for SUP7 steel obtained in axial loading are plotted as S-N diagram in Fig.8. Figure 8(a) indicates the results for T-450G and T-386 specimens, in which the fatigue limit for T-386 specimen is higher comparing with the result for T-450G specimen. In addition, the interior-induced fracture is easily caused in T-386G specimen having higher hardness similar to the trend in the case of rotating bending. Figure 8(b) is S-N diagram obtained for T-386 specimens in the respective series. The fatigue limit of each series is given as follows; T-386G

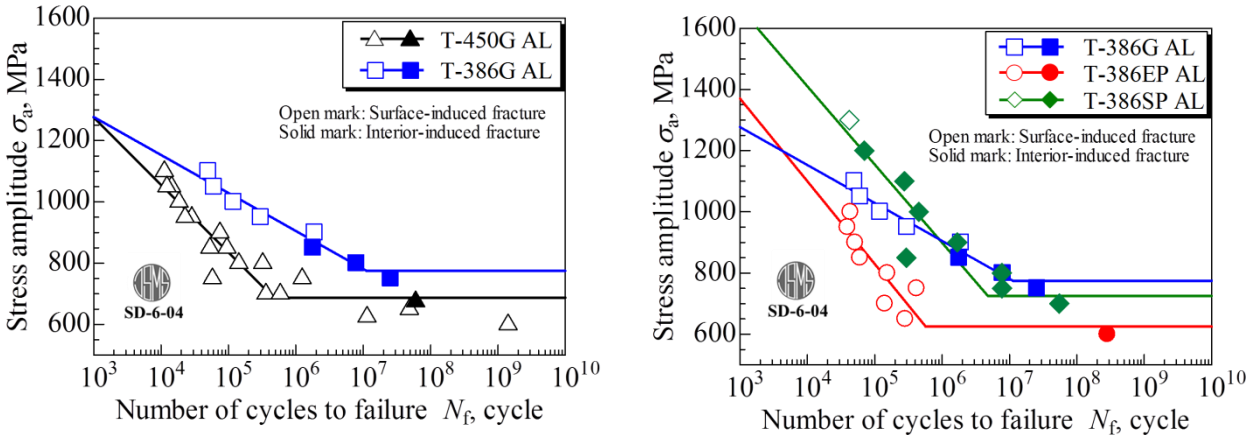

(a) T-450G series and T-386G series (b) Various series of T-386 specimens

Figure 8. S-N diagrams for SUP7 steel in axial loading

series: 775MPa, T-386EP series: 625MPa and T-386SP series: 725MPa, respectively. Variation of the fatigue limit and the fracture mode depending on the surface finishing is quite similar to the trend in the case of rotating bending.

Figure 9 indicates S-N diagram obtained for SWOSC-V steel in rotating bending. The fatigue limit for T-363G specimen is higher than that for T-395G specimen depending the hardness realized by the tempering at the respective temperatures. The interior-induced fracture was not observed even for the gigacycle regime in the case of low temperature tempering. The slope of the inclined portion in T-395G specimen is fairly steep comparing with that in T-363G specimen. Figure 10 is S-N diagram obtained for the respective series of T-386 specimens. The fatigue limit for T-363EP series is decreased due to the removal of the surface layer with the compressive residual stress. This trend is very common to the case of SUP7 steel as shown in Fig.7(b) and Fig.8(b).

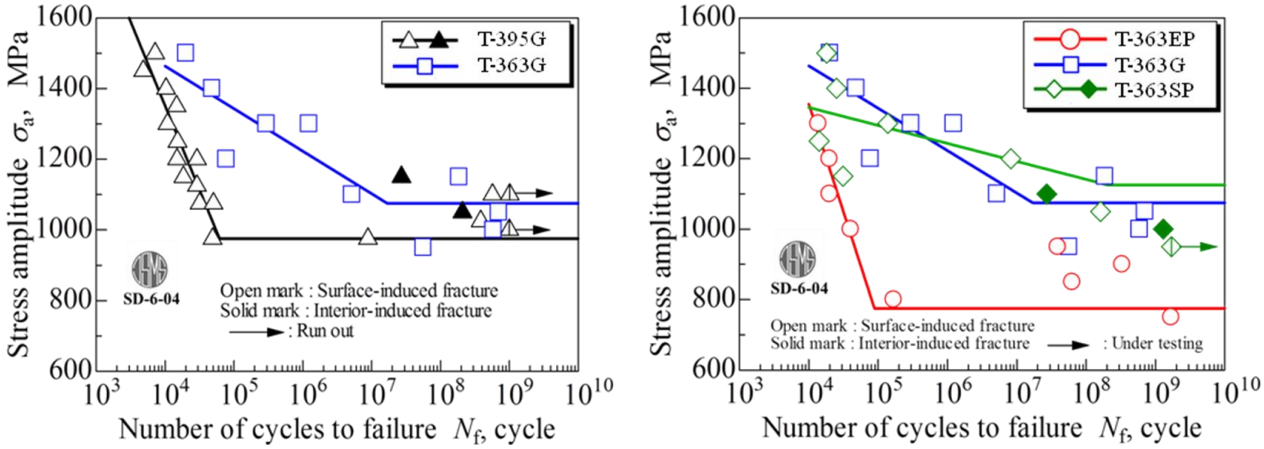

(a) T-395G series and T-363G series (b) Various series of T-363 specimens

Figure 9. S-N diagrams for SWOSC-V steel in rotating bending

3.3. SEM observations of fracture surface

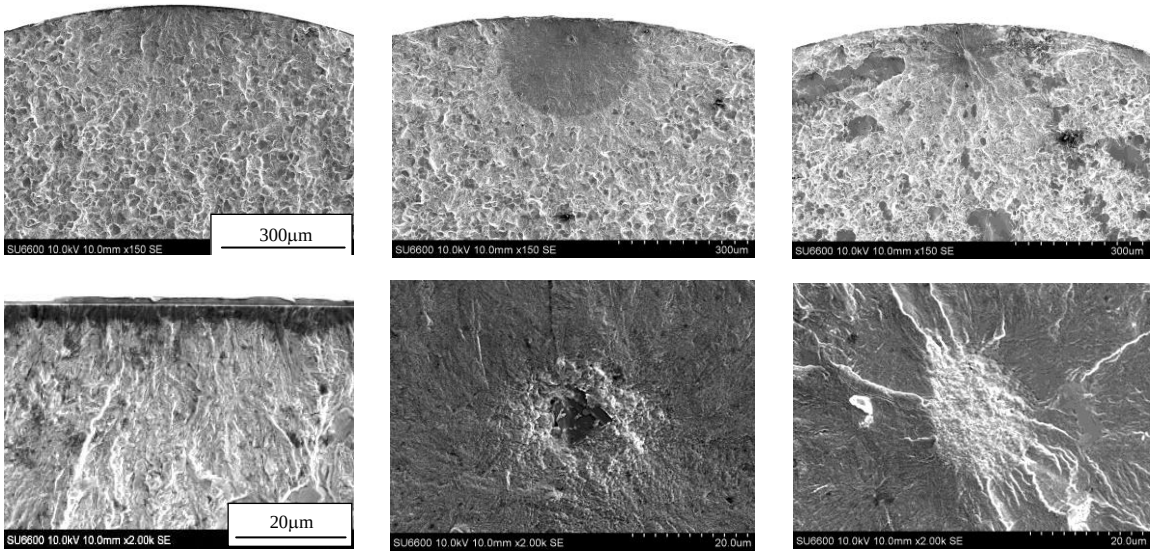

(a) Surface-induced fracture in rotating bending [$\sigma_a = 1400$ MPa, $N = 1.8\times10^4$]

(b) Interior-induced fracture in rotating bending [$\sigma_a = 950$ MPa, $N = 8.8\times10^8$]

(c) Interior-induced fracture in axial loading [$\sigma_a = 1200$ MPa, $N = 7.0\times10^4$]

Figure 11. Typical examples of fracture surfaces for SUP7 steel in both loading types

Fracture surface for T-386G specimen failed at $\sigma_a = 1400$ MPa with a short life of $N = 1.8 \times 10^4$ in rotating bending is shown in Fig.11(a), where the top is the result observed at low magnification and the bottom the result at high magnification. In this case, the fatigue crack took place on the specimen surface and it propagated inside the specimen. Figure 11(b) gives another example of the fracture surface at $\sigma_a = 950$ MPa with a life of $N = 8.8 \times 10^8$ in the interior-induced fracture modewith a clear fish-eye. In this case, the fatigue crack took place around the interior inclusion at the center of the fish-eye and the fine granular area[FGA] was found around the inclusion. These pairs of results give examples of the fracture surface in rotating bending. However, Fig. 11(c) gives other examples of the fracture surface at $\sigma_a = 700$ MPa with a life of $N = 7.7 \times 10^6$ in the interior-induced fracture mode in axial loading. No inclusion was found at the crack initiation site at the center of the fish-eye in this case, but the fine granular area[FGA] can be observed at the crack initiation site.

The fine granular area in Fig.11(c) was again carefully observed by inclining the sample ± 5deg., after which 3-D image of the fracture surface around the FGA was reconstructed by means of stereo-projection analysis[A Software of Mex supplied by Alicona Co. Ltd.]. Based on this analysis, it was found that a plane of the FGA inclined 60deg. against the macroscopic fracture surface and the gap of the local surface levels at both ends of the FGA is about 10 μm.

Several examples of fracture surfaces for SWOSC-V steel in rotating bending are indicated in Fig.12, in which the top is the result observed at low magnification and the bottom the result at high magnification. In the case of Fig.12(a), the fatigue crack took place at a shot-peened dimple on the specimen surface and it propagated inside the material resulting the final fracture. In Fig.12(b), the fine granular area[FGA] was formed at an interior site along a inclined plane. According to the stereo-projection analysis, this plane was inclined 60deg. against the macroscopic fracture surface similar to the previous result obtained for SUP7 steel. Figure 12(c) gives another example of the fracture surface in interior-induced fracture and a defect was found at the crack initiation site. However, any inclusion was not observed here regardless of careful EDS-analysis. Thus, no inclusion was found at the crack initiation site in every series of SWOSC-V steel. It is supposed that this fact comes from high cleanliness of the present steel.

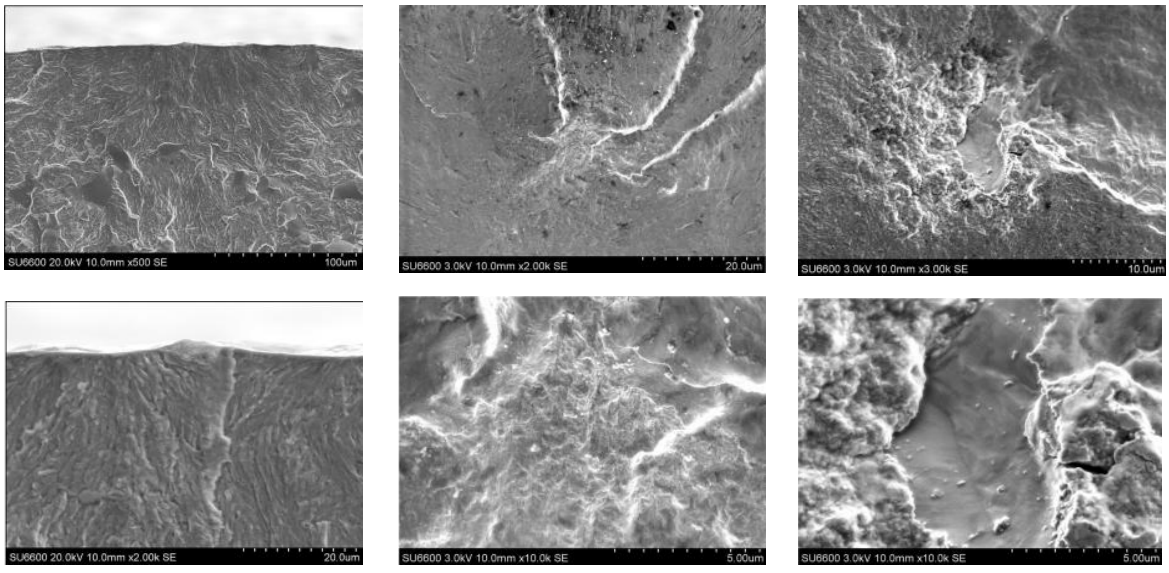

(a) Surface-induced fracture [$\sigma_a = 1050$ MPa, $N = 1.6 \times 10^8$] (b) Interior-induced fracture [$\sigma_a = 1100$ MPa, $N = 2.7 \times 10^7$] (c) Interior-induced fracture [$\sigma_a = 1050$ MPa, $N = 2.1 \times 10^8$]

Figure 12. Typical examples of fracture surfaces for SWOSC-V steel in rotating bending

3.4. Effects of loading type and residual stress on the fatigue property

Fatigue limits of the respective series of T-386 in both loading types are depicted in Fig.13, where values in the left hand side of each couple of the results are higher than the values in the right hand side. This aspect has been often reported for many kinds of metallic materials by many researchers. Thus, it was reconfirmed that the fatigue limit in rotating bending is a little higher than that in axial loading. It is another finding that the fatigue limit for T-386EP specimen is clearly lower than that for T-386G and T-386SP specimens. This can be attributed to the fact that the compressive residual stress is fully released by the electrochemical polishing. Figure 14 represents the difference of the crack initiation depth between both loading types for same fatigue test results as in Fig.13. The depth of crack initiation site for T-386EP specimen is almost same between both loading types, but the depth in axial loading is significantly deeper than that in rotating bending.

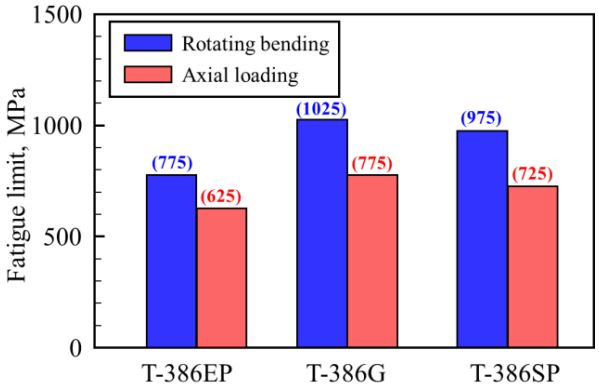

Figure 13. Difference of fatigue limits

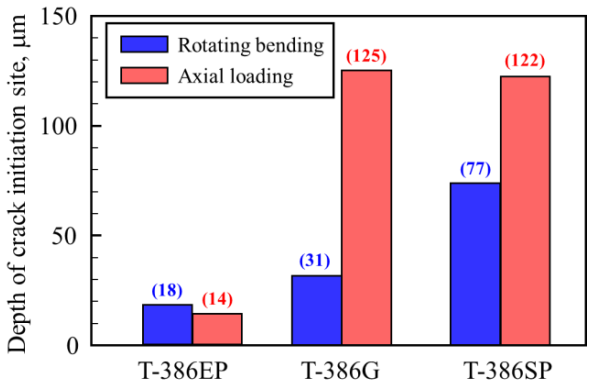

Figure 14. Difference of crack initiation depths

The fact that a significant difference of the crack initiation depth took place depending on the loading types can be well explained as follows; The stress distribution across the cross section in rotating bending has a significant gradient, while the stress distribution is uniform in axial loading as illustrated in Fig.15. In the case of rotating bending, the stress distribution has a steep slope and, therefore, the stress in the core portion is markedly lower than the outer layer. The crack is supposed to occur at higher stress region, but strength of the surface layer is improved by some kinds of surface treatments. In such a circumstance, the fatigue crack can occur at a definite

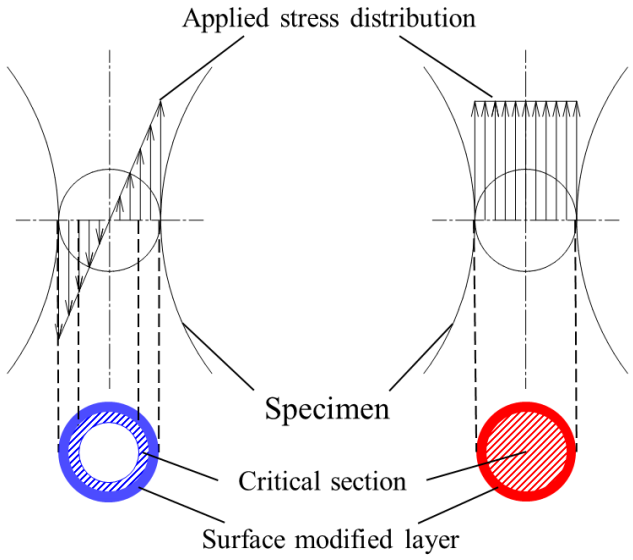

Figure 15. Schematics of stress distributions across the cross section in both loading types

ring-like area hatched in Fig.15. On the other hand, such an area occurring fatigue crack is the entire cross section without the modified surface layer having the improved strength in the case of axial loading. Thus, the critical volume participating in the fatigue crack initiation in axial loading is extremely larger than that in rotating bending. The fact that the crack initiation depth in axial loading is clearly higher than the results in rotating bending in Fig.14 can be well interpreted in this concept. In the case of high strength steels such as spring steel, material defects such as inclusion and machining flaws become sensitive to the crack initiation comparing with the usual structural steels with some moderate strength. Paying a particular attention to this aspect, the number of such defects in axial loading is much larger than the case in rotating bending. Therefore, the size of the most harmful defect in axial loading becomes larger than that in rotating bending. This is another reason why the fatigue limit in axial loading becomes a little lower than that in rotating bending.

4. Conclusions

In order to investigate the very high cycle fatigue properties of spring steels (SUP7 and SWOSC-V), fatigue tests were performed for specimens prepared by several different processes in both rotating bending and axial loading. Main conclusions obtained in this study are summarized as follows;

(1) In every series of the specimen preparation, fatigue fracture can occur in the very high cycle regime such as $10^7 - 10^9$ cycles regardless of the specimen's hardness, the surface roughness and the loading type.
(2) Fatigue limit in rotating bending is a little higher than that in axial loading for every series of specimens. This fact can be attributed to the difference of the stress distribution across the section, i.e. the critical volume participating in the crack initiation in axial loading is much larger than that in rotating bending.
(3) At higher stress levels with shorter life, the surface-induced fracture tends to occur instead of the interior-induced fracture, but the interior-induced fracture tends to occur at relatively higher stress levels in the case of shot-peened specimen due to suppression of crack initiation on the specimen surface by high value of the compressive residual stress.
(4) In the case of interior fracture mode for the conventional spring steel, an inclusion was usually found at the crack initiation site (Central portion of the fish-eye) and the FGA was observed around the inclusion. But, in the case of high cleanliness spring steel, such an inclusion was not found even in the interior fracture mode and a FGA-like facet inclined 60deg. against the macroscopic fracture surface was formed at the crack initiation site.

References

[1] A. Woehler, Uber die Festigkeits-Versuche mit Eisen und Stahl, Zeitschrift fur Bauwesen, 20, (1870), 74-106.
[2] K. Shiozawa, T. Sakai et al., Databook on Fatigue Strength of Metallic Materials, Vols. 1-3, Elsevier Science B. V. and JSMS, (1996).
[3] S. Mimura, T. Aoki, T. Sakakibara, M. Wakita, Development of High Fatigue-Proof Spring Using High Silicone Oil Tempered Wire, Transactions of the Japan Society of Spring Engineers, 46, (2001) , 1–6.
[4] T. Sakai, Review and Prospects for Current Studies on Very High Cycle Fatigue of Metallic Materials for Machine Structural Use, Journal of Solid Mechanics and Materials Engineering, 3(3), (2009), 425-439.
[5] T. Sakai, T. Furusawa, R. Takizawa, N. Oguma, H. Hohjo, H. Ikuno, Development of Multi-type High Efficiency Fatigue Testing Machines in Rotating Bending and Axial Loading, Proceedings of the Hael Mughrabi Honorary Symposium, TMS Annual Meeting, (2008), 69–73.
[6] T. Sakai et al., Standard Evaluation Method of Fatigue Reliability for Metallic Materials -Standard Regression Method of S-N Curves- [JSMS-SD-6-08], JSMS Committees on Fatigue and Reliability Engineering, (2008).